ELSEVIER

Precambrian Research 109 (2001) 1–23

Precambrian Research

www.elsevier.com/locate/precamres

Sr, Nd isotopes and geochemistry of the Bayuda Desert high-grade metamorphic basement (Sudan): an early Pan-African oceanic convergent margin, not the edge of the East Saharan ghost craton?

Dirk Küster [1], Jean-Paul Liégeois *

Section of Isotope Geology, Africa Museum, 3080 Tervuren, Belgium

Received 20 January 2000; accepted 30 October 2000

Abstract

The high-grade metamorphic basement of the Bayuda Desert is situated at the inferred transition between the juvenile Neoproterozoic mainly greenschist facies Arabian–Nubian Shield (ANS) and the pre-Neoproterozoic mainly amphibolite facies domain of the East Saharan Ghost Craton. New geochemical and Sr–Nd isotope data reveal that this basement in Bayuda constituted a Neoproterozoic oceanic convergent margin succession with limited and probably late input of old material. Within this series, garnet amphibolites and epidote–biotite gneisses have geochemical characteristics of HFSE-depleted tholeiitic basalts and low- to medium-K dacites and rhyodacites, indicating magmatism in an oceanic island arc or back-arc basin environment. This magmatism occurred at 806 ± 19 Ma (Sm–Nd 11 WR isochron), similar in age to arc magmatism in the ANS. Leucocratic gneisses, muscovite schists and garnet–biotite schists form the dominant meta-sedimentary rocks of the study area. They were primarily derived from two different sources: volcanogenic sediments from a Neoproterozoic island arc (T_{DM} Nd model ages between 790 and 900 Ma) and terrigeneous sediments from an older continental source (T_{DM} Nd model ages up to 2100 Ma). The volcanosedimentary succession was metamorphosed under amphibolite facies conditions prior to 670 Ma, probably at approximately 700 Ma. The high-grade metamorphism is related to a frontal collisional event that also produced syn-collisional peraluminous granites preserved as muscovite–biotite gneisses. Meta-igneous rocks from eastern Bayuda have ε_{Nd} values at 806 Ma of $+5.2 \pm 0.4$, indicating a less depleted mantle source (crustal contamination can be excluded) than the neighbouring Gabgaba–Gebeit terrane (ε_{Nd}, ca. $+7$) from the Arabian–Nubian shield. Less depleted mantle source is also known at Jebel Moya to the south, and inside the Arabian–Nubian Shield to the southeast of Bayuda. Lithological and structural similarities (dominantly northeast striking foliation) with the Bayuda Desert succession occur in many parts of central and western Sudan, suggesting a comparable geodynamic evolution. It is proposed that a Neoproterozoic oceanic convergent margin (Bayuda type succession) collided at approximately 700 Ma to the northwest with the East Saharan ghost craton, whose easternmost limit must lie below or more to the west than previously thought.

* Corresponding author.

E-mail addresses: dirk@geosys.bg.tu-berlin.de (D. Küster), jplieg@ulb.ac.be (J.-P. Liégeois).

[1] Present address: Florastrasse 13, 13187 Berlin, Germany. Fax: +49-30-31472837

0301-9268/01/$ - see front matter

PII: S0301-9268(00)00147-9

Keywords: NE Africa; Pan-African orogeny; Metamorphic rocks; Isotopes; Island arc; Geodynamical evolution

Keywords: HFSE, high field strength elements; REE, rare earth elements; LREE, light REE; MREE, medium REE; LILE, large ion lithophile elements; MORB, mid-ocean ridge basalts; AFM, $Na_2O + K_2O - FeOt - MgO$; A/CNK, Al2O3/CaO + Na2O + K2O; MSWD, mean square weighted deviate; WR, whole-rock; AFC, assimilation-fractional crystallization

1. Introduction

A major problem in the Precambrian geology of northern Africa is the unresolved history of a large tract of heterogeneous and poorly known continental crust in the central-eastern part of the Sahara and southerly adjoining parts of the Sahel. This tract of Precambrian basement stretches between the Tuareg Shield (Hoggar-Aïr) in the west, the Arabian–Nubian Shield in the east and the Congo Craton in the south. To the north, it disappears beneath thick Phanerozoic strata of the African continental margin (Fig. 1). Common features of the rocks comprise a predominance of high-grade gneissic, often migmatitic, lithologies as well as isotopic evidence of both pre-Neoproterozoic crust formation and large-scale Neoproterozoic remobilisation (Harms et al., 1990; Black and Liégeois, 1993; Stern, 1994).

This domain is widely referred to as the East Saharan Craton (Kröner, 1979; Schandelmeier et al., 1987; Greiling et al., 1994; Stern et al., 1994) or as the Nile craton (Abdelsalam et al., 1998). However, this terminology is misleading mainly because of its dominant Pan-African imprint (Schandelmeier et al., 1990; Abdel Rahman et al., 1991; Black and Liégeois, 1993; Stern et al., 1994). This has led Black and Liégeois (1993) to propose the concept of the 'East (or Central) Saharan Ghost Craton' (ESGC), indicating the existence of a craton to the east of the Tuareg shield before 700 Ma (Liégeois et al., 1994), but at least partially remobilised (decratonisation through lithospheric mantle delamination; Black and Liégeois, 1993) during the Neoproterozoic. In this paper, we will adopt the ESGC term to refer to the crystalline basement already described, knowing that neither its extent nor nature is yet determined. We consider here that the Pan-African orogeny is the Neoproterozoic orogeny that led to the Pangaea supercontinent, including subduction, collision and post-collision periods (Liégeois, 1998), excluding events such as continent break-off or passive margin sedimentation (referred to in this case as Neoproterozoic). Taking into account the very wide area affected by the Pan-African orogeny, diachronisms are inevitable. In the eastern Tuareg shield, Liégeois et al., 1994 have defined an early Pan-African (750–660 Ma) and a late Pan-African (650–580 Ma) phase. If the entire Tuareg shield is considered, early isolated accretion events occurred as soon as 900–850 Ma and latest localized movements as late as 525 Ma (Black et al., 1994; Liégeois et al., 2000).

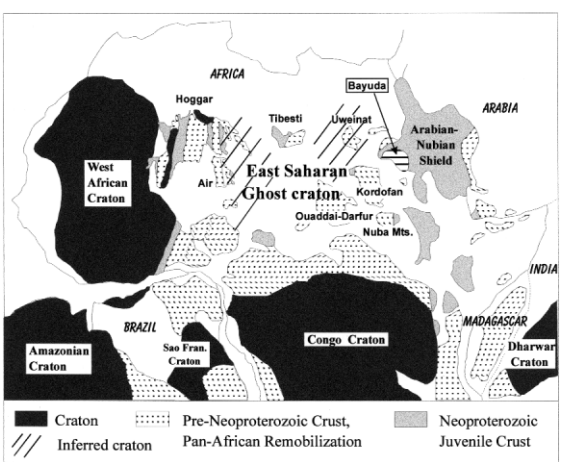

Fig. 1. Geological sketch map of northern Africa. The position of the Bayuda Desert is indicated by an arrow.

The only part currently known of the ESGC that has an undisturbed Archaean to Palaeoproterozoic history is the small fragment exposed in the Uweinat inlier (Fig. 1; Klerkx and Deutsch, 1977; Sultan et al., 1994). In addition, on its western part, the ESGC behaved rheologically as a craton during the Pan-African orogeny (Liégeois et al., 1994, 2000). Near the southern and eastern boundaries of the ESGC (Cameroon, Centrafrican Republic, Sudan), records of the pre-Neoproterozoic evolution have largely been obliterated by Pan-African

(800–550 Ma) pervasive metamorphism, intense deformation and widespread granitoid emplacement (Pin and Poidevin, 1987; Harms et al., 1990; Toteu et al., 1990; Stern et al., 1994). Beside Neoproterozoic remobilisation, there is also growing evidence in these areas of Neoproterozoic juvenile crust formation (Rogers et al., 1978; Toteu et al., 1990; Pinna et al., 1994) and of Neoproterozoic rifting and oceanic basin development (Schandelmeier et al., 1990; Abdel Rahman et al. 1991; Pinna et al., 1994; Schandelmeier et al., 1994). The ESGC may have been a coherent continental block prior to the Neoproterozoic, when it became subjected to extensional tectonics, rifting, oceanic basin development and subsequent basin closure and collision (cf. Schandelmeier et al., 1994). Alternatively, the ESGC may have been at least partly assembled during the Neoproterozoic from 'exotic' terranes of different ancestry, as proposed for the Tuareg Shield located just to the west of the ESGC (Fig. 1; Black et al., 1994; Liégeois et al., 1994), dismissing the cratonic character of these areas. We emphasise that the heart of the ESGC is very poorly known.

On its eastern side, the ESGC is bounded by the Arabian–Nubian shield (ANS). The ANS was likewise assembled from a number of terranes; however, all of these are made up of juvenile Neoproterozoic crust. Rock associations in the ANS are predominantly in greenschist facies. Towards the ESGC, they pass into high-grade metamorphic lithologies. This change in metamorphic grade has been interpreted as indicating a pre-Pan-African origin of the high-grade rocks and their assignment to a pre-Neoproterozoic craton (The East Saharan or Nile Craton). The boundary between the two metamorphic provinces coincides approximately with the course of River Nile in Sudan and Egypt.

In this paper, we present results of geochemical and isotopic investigations on high-grade metamorphic lithologies from the Bayuda Desert in north central Sudan adjacent to the Arabian–Nubian Shield (Fig. 1). We use these data to interpret the Neoproterozoic geodynamical evolution of the Bayuda region and discuss its implications for the ESGC history.

2. Geological outline of the Bayuda Desert and surroundings

The Bayuda Desert is situated inside the Great Bend of the River Nile in northern Sudan (Fig. 2) and constitutes the southern part of the Bayuda terrane (Schandelmeier et al., 1994). This terrane consists of high-grade metamorphic rocks and is bordered by the Halfa terrane in the northwest and by the Gabgaba terrane in the east (Fig. 2). The Gabgaba terrane is part of the ANS, being composed of low-grade metamorphic juvenile Neoproterozoic island arc/back arc basin assemblages. The Halfa terrane contains both juvenile Neoproterozoic crust and high-grade gneisses with pre-Pan-African crustal heritage (Stern et al., 1994). The terranes were assembled during several phases of deformation between about 750 and 580 Ma related to generally northwest–southeast (NW/SE) directed convergence (Abdelsalam and Stern, 1996).

2.1. Structural and geochronological framework

It has been considered that the Halfa and Bayuda terranes were contiguous parts of the ESGC prior to Neoproterozoic times, but were separated by rifting at about 830 Ma (Schandelmeier et al., 1994; Abdelsalam et al., 1995, 1998). The rift would have evolved into an oceanic re-entrant and eventually developed a NW-dipping subduction zone with an Andean-type (Stern et al., 1994) or intra-oceanic (Harms et al., 1994) magmatic arc on the southern margin of the Halfa terrane. Continuing subduction led to collision between the Halfa and Bayuda terranes at 750–700 Ma (Abdelsalam et al., 1995) and resulted in emplacement of the greenschist arc assemblage upon the Bayuda terrane as south (S)- to SE-verging nappes. Ophiolitic remnants of the nappes define the northeast (NE)- to east (E)-trending Delgo (or Atmur-Delgo) suture, and make the boundary between the 're-united' Halfa and Bayuda terranes (Fig. 2). Dominantly NE- to E-trending relict fold structures in the Bayuda Desert, often with horizontal axial planes (El Rabaa, 1976; Barth and Meinhold, 1979), probably originated from this collision. Collision-re-

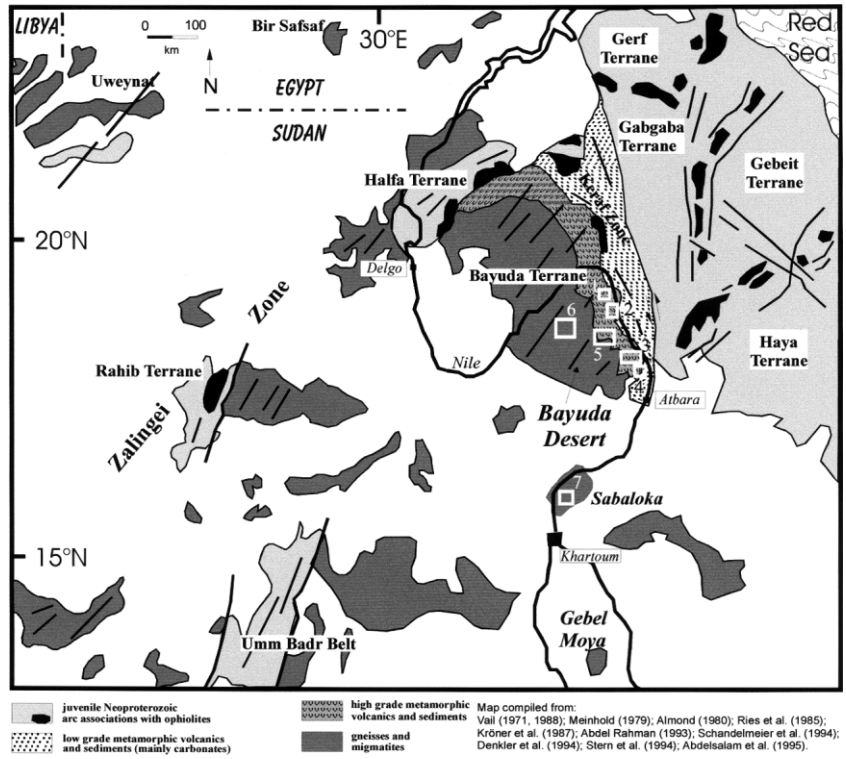

Fig. 2. Geological sketch map of the Bayuda Desert and surrounding areas showing major lithostructural units and working areas: 1, Jebel Absol; 2, Khor Dam Et Tor; 3, Wadi Kurmut/Jebel Kurbei; 4, Wadi Abu Harik; 5, Khor El Had; 6, El Melagi/Wadi Umm Tundiba; 7, SE of Querri station. The boundary between the gneisses and migmatites and the metavolcanosedimentary unit in the Bayuda Desert largely follows Vail (1988). Post-tectonic and anorogenic granitoids are omitted on the map.

lated granulite to amphibolite facies metamorphism in the region occurred between 720 and 700 Ma (Kröner et al., 1987; Harms et al., 1994; Stern et al., 1994).

The contact between the Gabgaba terrane and the Bayuda terrane is marked by the Keraf suture zone $\sim$50 km wide and $\sim$500 km long, N–S oriented (Fig. 2; Abdelsalam et al., 1995, 1998). This zone is structurally dominated by N-trending upright folds in the north, and by N- and NNW-trending sinistral strike slip faults in the south. Keraf structures truncate or refold earlier E- to NE-trending folds and thrusts in the eastern Bayuda Desert. Keraf deformation is interpreted to reflect sinistral transpression related to NW–SE oblique convergence between the Gabgaba and Bayuda terranes (Abdelsalam et al., 1998). However, its age and significance are not yet fully constrained. Recent research (Bailo, 2000) shows that early thrusting along the Keraf suture is older than 710 Ma (the age of discordant granite plutons), while sinistral shear movements lasted from 640 to 580 Ma (Abdelsalam et al., 1998). The cessation of Keraf movements (approximately 580 Ma) corresponds to the age of discordant post-kinematic granitoid plutons in the whole region including Bayuda (cf. Küster and Harms, 1998) and to the cooling stage of high-temperature metamorphism in the Delgo (Denkler et al., 1994; Harms et al., 1994) and Sabaloka (Kröner et al., 1987) areas. This age marks the end of Pan-African orogenic evolution in the area.

2.2. High-grade metamorphic lithologies of the Bayuda Desert

To highlight first-order lithological differences, we have subdivided the high-grade metamorphic

rocks of the Bayuda Desert into two geographical units (Fig. 2), adopting largely the division and boundaries of Vail (1971, 1988).

1. A monotonous migmatised series of mainly granitoid gneisses and subordinate amphibolites in western and central Bayuda (the 'grey gneisses' of Vail), in this paper referred to as the gneiss–migmatite unit (GM unit). Migmatitic gneisses occur also in the Sabaloka inlier (Almond, 1980) approximately 200 km south of the Bayuda Desert (Fig. 2) and are included in this group.
2. A heterogeneous non-migmatised succession of felsic gneisses, amphibolites, various schists, quartzites and marbles in eastern Bayuda (Vail's 'meta-sedimentary group'), in this paper referred to as the metavolcanosedimentary unit (MVS unit).

Vail (1979, 1988) interpreted his 'grey gneisses' as a polymetamorphosed pre-Pan-African continental crust, forming a basement to the meta-sedimentary group, considered as shelf deposits.

Metamorphic conditions of the GM unit are generally in the upper amphibolite facies; patches of relict granulite facies are preserved in the Sabaloka basement. There, Kröner et al. (1987) dated the granulite facies metamorphism (600–800°C and 6–8 kbar) at approximately 700 Ma, and the retrograde migmatitisation under amphibolite facies conditions at approximately 570 Ma. In the Bayuda Desert, age and pressure–temperature conditions of amphibolite facies metamorphism and migmatisation are not known, but semi-concordant late-kinematic pegmatite bodies from the Rahaba mine (between El Melagi and Khor Dam Et Tor; Fig. 2), constituting a minimum age for the migmatitisation, have been dated at 675 Ma (Küster, 1995). Migmatite formation in the Bayuda Desert may have been largely coeval with granulite formation and 100 Ma older than retrogressive migmatisation at Sabaloka.

The MVS unit is generally metamorphosed in the medium to upper amphibolite facies, and is characterised by kyanite and garnet in metapelites and hornblende, and garnet and pyroxene in amphibolites (El Rabaa, 1976). T_{DM} Nd model ages from a few samples of the MVS unit yielded crustal residence ages between 1000 and 1600 Ma (Harris et al., 1984) and indicate participation of the pre-Neoproterozoic crust in the sedimentary source. Barth and Meinhold (1979), Meinhold (1979) have proposed a shallow water shelf-like environment for one part of the succession (their 'Kurmut Series'), but suggested an island arc affinity for another part (their 'Absol Series'). Both Vail (1979, 1988), Meinhold (1979) suggested a pre-Pan-African age of deposition for the high-grade rocks of the eastern Bayuda Desert.

Low-grade volcanic rocks from the Keraf zone are known in the northeasternmost Bayuda desert and are similar in age ($\sim$800 Ma) and composition to arc-derived metavolcanic rocks of the ANS (Ries et al., 1985). A back-arc environment has been proposed for the central Keraf zone (Abdel Rahman, 1993). In the northern Keraf, a carbonate-dominated sedimentary sequence is considered to be deposited at around 750 Ma on the eastern flank of the passive margin of the East Saharan Craton (Stern et al., 1993).

3. Analytical techniques

We sampled characteristic lithologies representing both GM and MVS units from a number of localities in eastern, central and western Bayuda Desert (Table 1 and Fig. 2). Additional samples were taken for comparison at Sabaloka where a deeper crustal section is exposed.

The geochemical and isotopic results are shown in Tables 2 and 3. Major elements were determined by X-ray fluorescence (XRF) at Technische Universität Berlin. Trace elements were analysed by inductively coupled plasma-mass spectrometry (ICP-MS) in the Geochemical Laboratory of the Africa Museum in Tervuren, except Sr, Ni and Cr that were analysed by XRF in Berlin.

Sr- and Nd-isotope analyses were carried out in the isotopic geology laboratory of the Africa Museum. Samples were dissolved into a suboiled $HF–HNO_3$ acid mixture. If a solid phase remained after centrifugation, it was again dissolved into the same acid mixture but into teflon-lined stainless-steel digestion vessels at 180°C. After Sr and Nd separation on ion-exchange resins, Sr isotopic compositions were measured on a single

Ta filament and Nd isotopic compositions on a triple Ta–Re–Ta filament using a Micromass Sector 54 mass spectrometer. Repeated measurements of Sr and Nd standards have shown that the between-run error is better than $\pm 0.000\,015$. The NBS987 standard yields a value for $^{87}Sr/^{86}Sr$ of $0.710\,252 \pm 0.000\,010$ (2σ on the mean of 20 standards measured together with the samples, normalised to $^{86}Sr/^{88}Sr = 0.1194$), and the MERCK Nd standard yields a value for $^{143}Nd/^{144}Nd$ of $0.511\,738 \pm 0.000\,008$ (2σ on the mean of 20 standards measured together with the samples, normalised to $^{146}Nd/^{144}Nd = 0.7219$, and corresponding to a La Jolla standard value of 0.511 866). Rb and Sr concentrations were measured by X-ray fluorescence or by isotope dilution when concentrations were < 10 p.p.m. The error on the Rb/Sr ratio is $< 4\%$. Sm and Nd concentrations were measured by ICP-MS. The error on the Sm/Nd ratio is $< 4\%$. The Rb–Sr and Sm–Nd ages were calculated following Ludwig (1999). The decay constants used were 1.42×10^{-11} a^{-1} (^{87}Rb) and 6.54×10^{-12} a^{-1} (^{147}Sm). Sr and Nd isotope ratios are presented in Table 3.

Table 1
Localities and sampled lithologies

Locality	Area (Fig. 2)	Rock	Protolith
Eastern Bayuda			
Northern part of MVS unit			
Jebel Absol	Area 1	Amphibolite	Tholeiitic basalt
Khor Dam Et Tor	Area 2	Amphibolite	Tholeiitic basalt
		Garnet amphibolite	Tholeiitic basalt
		Quartz amphibolite	Calc-alkaline andesite
		Biotite–epidote orthogneiss	Calc-alkaline rhyodacite
		Biotite–muscovite orthogneiss	S-Type granite
Southern part of MVS unit			
Wadi Kurmut	Area 3	Quartz–muscovite schist	Arkose
		Quartz–feldspar gneiss	Sandstone
		Garnet amphibolite	Tholeiitic basalt
		Biotite paragneiss	Graywacke
		Pyroxene amphibolite	Tholeiitic basalt
E Jebel Kurbei	Area 3	Garnet–staurolite–kyanite schist	Shale
Wadi Abu Harik	Area 4	Biotite–epidote orthogneiss	Calc-alkaline rhyodacite
Central Bayuda			
Boundary region between MVS and GM units			
Khor El Had	Area 5	Muscovite paragneiss, garnet–biotite schist	Arkose, graywacke
Western Bayuda			
GM unit			
El Melagi	Area 6	Biotite–muscovite orthogneiss	S-Type granite
Wadi Umm Tundiba	Area 6	Amphibolite	Tholeiitic basalt
Sabaloka			
GM unit			
SE Querri station	Area 7	Garnet-cordierite gneiss	Graywacke

Table 2
Geochemical analyses of high-grade metamorphic rocks from the Bayuda Desert

	Amphibolites												
	Khor Dam Et Tor					Jebel Absol			Wadi Kurmut		Wadi Umm Tundiba		
	9-2b	9-2a	11-3	9-5	11-1	10-1a	10-5b	10-5a	6-2a	6-2b	6-4	12-6	12-4a
wt.%													
SiO_2	51.25	48.84	46.51	50.97	53.60	48.67	49.60	50.13	48.62	52.28	43.30	49.31	48.94
Al_2O_3	5.63	9.43	13.15	13.71	17.15	10.59	14.58	19.09	17.62	14.93	18.84	16.32	15.19
Fe_2O_3	8.44	9.95	11.09	13.02	9.02	9.59	6.68	8.07	13.85	11.05	15.92	6.81	10.38
MnO	0.17	0.17	0.19	0.20	0.13	0.17	0.13	0.15	0.15	0.30	0.17	0.13	0.16
MgO	15.25	13.00	10.09	7.15	4.24	13.57	10.25	6.36	7.89	6.71	7.66	10.77	9.18
CaO	16.12	14.06	13.50	12.05	8.28	15.43	16.69	14.22	10.26	13.19	11.12	15.69	13.92
Na_2O	0.84	1.31	1.78	2.09	1.84	0.89	1.10	1.94	0.43	0.16	1.31	0.47	1.19
K_2O	0.15	0.19	0.20	0.05	1.65	0.05	0.08	0.10	0.10	0.05	0.07	0.10	0.13
TiO_2	0.52	0.94	0.72	1.26	1.34	0.52	0.39	0.62	0.83	0.70	0.81	0.27	0.74
P_2O_5	0.10	0.06	0.07	0.14	0.41	0.06	0.04	0.08	0.13	0.15	0.03	0.03	0.08
LOI	2.18	2.47	3.53	0.50	3.10	1.22	1.51	0.96	1.10	1.63	1.80	1.19	1.07
Total	100.65	100.42	100.82	101.14	100.76	100.76	101.05	101.71	100.98	101.14	101.03	101.09	100.98
p.p.m.													
Sr	93	241	116	64	777	64	95	130	471	295	180	139	151
Ba	36	44	61	9	488	9	9	21	24	19	76	22	61
Rb	0	1	2	1	24	1	5	2	0	0	0	1	2
Zr	22	22	47	61	200	23	15	34	17	17	4	8	31
Y	10	15	16	23	35	12	10	14	12	11	3	7	14
V	195	282	265	244	178	209	196	202	248	270	735	154	249
Cr	1354	1010	434	51	31	947	446	37	208	295	15	418	333
Ni	161	113	181	71	23	253	158	61	64	86	15	217	144
Th	0.17	0.21	0.25	0.38	2.55	0.11	0.06	0.19	0.16	0.11	0.03	0.03	0.10
Hf	0.73	0.90	1.22	2.01	4.62	0.70	0.49	0.97	0.62	0.54	0.16	0.28	0.89
Nb	0.32	0.44	1.34	2.98	5.20	0.87	0.43	1.43	0.24	0.39	0.10	0.18	1.19
Ta	0.01	0.02	0.09	0.17	0.31	0.06	0.02	0.09	0.02	0.01	0.01	0.01	0.08
La	2.06	1.86	1.91	3.49	24.77	0.98	0.55	1.84	1.68	0.89	0.03	0.23	1.38
Ce	4.95	5.98	5.01	9.59	57.08	3.13	1.91	4.79	3.88	2.63	0.14	0.78	3.75
Pr	0.96	1.34	0.88	1.60	7.56	0.56	0.36	0.81	0.73	0.55	0.08	0.22	0.72
Nd	5.55	8.29	4.95	9.17	32.54	3.20	2.37	4.36	4.49	3.31	0.70	1.55	4.18
Sm	1.82	2.79	1.64	2.93	6.85	1.19	0.91	1.44	1.56	1.21	0.25	0.61	1.44
Eu	0.58	0.93	0.69	1.07	1.98	0.45	0.40	0.65	0.81	0.54	0.15	0.31	0.60
Gd	1.88	3.03	2.15	3.72	6.51	1.67	1.31	1.98	2.08	1.61	0.39	0.93	1.93
Dy	1.78	2.71	2.57	4.46	5.99	1.98	1.63	2.35	2.48	1.84	0.52	1.17	2.34
Ho	0.37	0.56	0.59	0.97	1.27	0.45	0.36	0.53	0.53	0.42	0.13	0.26	0.53
Er	0.95	1.39	1.65	2.76	3.31	1.25	1.02	1.47	1.50	1.15	0.36	0.73	1.45
Yb	0.86	1.20	1.65	2.51	3.13	1.20	0.98	1.45	1.33	1.18	0.37	0.74	1.45
Lu	0.12	0.17	0.24	0.37	0.46	0.18	0.14	0.21	0.18	0.18	0.05	0.10	0.21

Table 2 (*Continued*)

	Epidote–biotite gneisses						Muscovite–biotite gneisses					
	Wadi Abu Harik			K. Dam Et Tor		Wadi Kurmut	El Melagi					Khor El Had
	8-1	8-2	8-3	11-2a	9-1	6-3	12-3	12-5a	12-2	12-5B	12-1B	14.9
wt.%												
SiO_2	63.77	67.26	70.98	65.88	72.42	72.04	73.31	73.94	74.09	74.10	73.17	74.09
Al_2O_3	16.55	14.95	14.52	16.81	16.68	14.65	14.02	13.72	13.95	14.01	14.68	14.12
Fe_2O_3	5.08	4.57	3.24	4.28	2.06	2.00	2.22	2.13	1.83	0.71	0.49	1.24
MnO	0.09	0.08	0.07	0.07	0.06	0.03	0.04	0.04	0.04	0.02	0.03	0.07
MgO	2.18	1.74	1.39	1.59	0.66	0.94	0.47	0.41	0.42	0.18	0.12	0.23
CaO	5.92	4.46	3.28	4.78	3.95	1.99	0.95	1.12	1.14	0.84	0.82	0.94
Na_2O	3.86	2.76	3.55	4.07	4.80	4.26	2.29	3.17	3.23	3.25	3.74	3.35
K_2O	1.51	2.88	2.53	1.55	0.60	2.82	5.58	4.26	4.34	5.71	4.76	3.41
TiO_2	0.49	0.43	0.34	0.50	0.21	0.33	0.32	0.26	0.25	0.08	0.05	0.11
P_2O_5	0.19	0.13	0.10	0.21	0.08	0.08	0.31	0.26	0.26	0.11	0.03	0.18
LOI	0.76	1.31	0.77	0.46	0.69	0.97	0.88	0.93	0.89	0.50	0.96	1.13
Total	100.40	100.57	100.76	100.19	102.21	100.11	100.39	100.24	100.44	99.51	98.86	98.87
p.p.m.												
Sr	586	355	330	564	493	300	51	47	49	73	82	73
Ba	288	418	399	349	301	400	315	182	184	308	156	156
Rb	32	65	59	27	9	93	283	251	253	251	247	224
Zr	84	129	108	131	70	99	130	139	94	42	28	61
Y	15	15	13	9	4	7	25	18	17	9	8	21
V	109	82	58	63	20	34	16	13	11	2	1	4
Cr	7	7	5	2	1	28	0	0	1	10	10	10
Ni	15	10	9	6	1	9	0	0	1	8	0	8
Th	1.85	1.30	3.22	0.83	0.35	11.58	12.10	9.15	8.57	3.76	4.56	6.10
Hf	2.68	3.77	3.57	3.33	1.92	3.26	3.82	4.04	2.94	1.58	1.28	2.37
Nb	1.97	2.18	1.97	2.23	0.82	13.94	9.40	9.15	8.69	4.22	8.58	13.07
Ta	0.15	0.14	0.20	0.15	0.04	1.15	1.11	1.27	1.24	0.87	2.03	1.00
La	9.71	7.26	5.57	5.31	3.16	19.15	21.66	18.38	16.55	7.79	6.19	12.66
Ce	23.33	18.15	13.83	10.85	6.95	32.95	48.72	40.84	36.37	16.02	12.60	26.54
Pr	3.20	2.67	2.01	1.48	1.01	3.43	6.11	5.02	4.45	1.84	1.38	2.99
Nd	13.85	11.71	8.84	6.81	4.41	10.42	23.29	19.39	17.34	6.34	3.87	9.97
Sm	3.01	2.57	2.00	1.55	0.86	1.61	5.46	4.72	3.90	1.28	0.96	2.30
Eu	0.78	0.62	0.49	0.62	0.42	0.42	0.47	0.48	0.48	0.41	0.18	0.25
Gd	2.68	2.33	2.03	1.54	0.75	1.46	4.79	4.12	3.44	1.38	0.92	2.58
Dy	2.36	2.36	2.02	1.44	0.66	1.08	4.50	3.53	3.15	1.55	1.01	3.24
Ho	0.51	0.52	0.45	0.31	0.14	0.21	0.86	0.59	0.59	0.28	0.22	0.71
Er	1.37	1.41	1.30	0.82	0.38	0.55	2.13	1.34	1.47	0.69	0.75	1.93
Yb	1.56	1.51	1.41	0.84	0.45	0.55	1.99	1.17	1.45	0.58	1.08	2.23
Lu	0.24	0.22	0.24	0.12	0.07	0.08	0.29	0.17	0.21	0.06	0.15	0.29

Table 2 (*Continued*)

	Meta-sediments		Jebel Khor			
	Khor El Had	Sabaloka	Wadi Kurmut		Kurbei	Dam Et Tor
	Ga-bi schist	Ga-cd schist	Na qtz felds gneiss	Impure quartzite	Ga bi st ky schist	Ms schist
	14-11	17-6	6-5	6-8B	7-1	11-2b
wt.%						
SiO_2	71.51	70.87	76.37	79.82	63.68	74.08
Al_2O_3	12.31	13.97	11.98	9.97	17.23	14.71
Fe_2O_3	6.12	5.31	3.03	2.50	6.86	0.60
MnO	0.09	0.09	0.06	0.02	0.10	0.02
MgO	2.08	2.21	0.51	0.55	3.05	0.22
CaO	1.12	1.27	2.47	0.09	2.15	1.05
Na_2O	1.15	1.98	4.55	0.10	2.89	3.71
K_2O	3.18	2.58	0.17	3.41	2.28	4.09
TiO_2	0.80	0.68	0.18	0.16	0.77	0.03
P_2O_5	0.17	0.08	0.07	0.02	0.25	0.07
LOI	1.61	0.81	1.66	2.11	1.25	0.93
Total	100.15	99.84	101.05	98.75	100.51	99.51
p.p.m.						
Sr	92	80	155	14	314	48
Ba	556	464	118	602	476	155
Rb	141	119	1	83	47	28
Zr	367	363	86	288	120	29
Y	32	61	47	56	30	16
V	90	86	1	9	115	6
Cr	66	86	1	9	44	0
Ni	30	26	1	7	28	0
Th	18.50	11.77	1.76	3.42	2.23	0.97
Hf	9.51	9.68	3.06	7.73	3.42	1.71
Nb	13.80	9.37	2.99	11.92	3.28	3.43
Ta	1.11	0.54	0.16	0.66	0.52	0.36
La	44.97	33.55	9.77	39.37	14.95	3.54
Ce	96.32	74.27	19.71	74.61	31.95	7.70
Pr	10.83	9.14	3.22	11.51	5.10	1.10
Nd	40.47	37.72	16.22	43.27	23.37	4.64
Sm	7.39	8.26	4.86	9.08	5.56	1.53
Eu	1.09	1.49	1.11	1.60	1.34	0.11
Gd	5.91	7.98	5.97	9.12	5.29	1.80
Dy	5.47	9.16	8.21	8.48	4.95	2.22
Ho	1.17	2.19	1.93	1.80	1.09	0.48
Er	3.04	6.34	5.86	4.74	2.90	1.36
Yb	3.06	6.80	5.93	4.90	2.96	1.60
Lu	0.45	1.02	0.92	0.73	0.45	0.23

Table 3
Isotopic data of high-grade metamorphic rocks from the Bayuda Desert[a]

	Rb	Sr	$^{87}Rb/^{86}Sr$	$^{87}Sr/^{86}Sr$	2σ	Sr_i at 806 Ma	Sm	Nd	$^{147}Sm/^{144}Nd$	$^{143}Nd/^{144}Nd$	2σ	$^{143}Nd/^{144}Nd$ at 806 Ma	ε_{Nd} at 806 Ma	T_{DM} (Ma)
Amphibolites														
12-4a	2.05	151	0.0393	0.708 912	0.000 010	0.708 460	1.44	4.18	0.2084	0.512 979	0.000 014	0.511 878	+5.5	–
12-6	1.04	139	0.0217	0.708 514	0.000 009	0.708 264	0.61	1.55	0.23817	0.513 130	0.000 009	0.511 872	+5.3	–
6-2a	0.14	471	0.0008	0.703 929	0.000 008	0.703 919	1.56	4.49	0.2102	0.512 975	0.000 012	0.511 864	+5.2	–
10-5a	2.06	130	0.0458	0.704 332	0.000 013	0.703 804	1.44	4.36	0.1998	0.512 911	0.000 007	0.511 855	+5.0	–
10-1a	1.05	64	0.0475	0.705 476	0.000 013	0.704 930	1.19	3.2	0.2249	0.513 044	0.000 012	0.511 855	+5.0	–
9-5	1.08	64	0.0488	0.704 281	0.000 008	0.703 719	2.93	9.17	0.1933	0.512 884	0.000 007	0.511 863	+5.2	–
9-2a	0.52	241	0.0062	0.703 127	0.000 010	0.703 055	2.79	8.29	0.2036	0.512 931	0.000 015	0.511 855	+5.0	–
11-1	24.2	777	0.0901	0.704 259	0.000 008	0.703 221	6.85	32.54	0.1273	0.512 535	0.000 008	0.511 862	+5.2	903
Epidote–biotite gneisses														
9-1	9.41	493	0.0552	0.703 456	0.000 008	0.702 821	0.86	4.41	0.1181	0.512 510	0.000 011	0.511 886	+5.6	858
11-2a	27.2	564	0.1395	0.704 277	0.000 008	0.702 672	1.55	6.81	0.1376	0.512 598	0.000 012	0.511 871	+5.3	899
6-3	89.0	300	0.8588	0.711 177	0.000 009	0.701 292	1.61	10.42	0.09364	0.512 348	0.000 011	0.511 853	+5.0	888
Muscovite–biotite gneisses														
12-3	259	51	14.9580	0.888 458	0.000 011	0.716 278	5.46	23.29	0.1418	0.511 903	0.000 008	0.511 154	−8.7	2427
12-2	253	49	15.2366	0.891 699	0.000 011	0.716 311	3.90	17.34	0.1361	0.511 910	0.000 009	0.511 191	−8.0	2229
12-5b	242	73	9.6957	0.816 103	0.000 013	0.704 496	1.28	6.34	0.1219	0.511 813	0.000 009	0.511 169	−8.4	2041
14-9	211	73	8.4328	0.790 800	0.000 009	<0.7	2.30	9.97	0.1393	0.512 026	0.000 008	0.511 290	−6.0	2084
Meta-sedimentary rocks														
11-2b	26.0	48	1.5689	0.717 021	0.000 009	<0.7	1.53	4.64	0.2001	0.512 839	0.000 007	0.511 781	+3.6	–
6-5	0.67	155	0.0125	0.703 914	0.000 011	0.703 770	4.86	16.22	0.1812	0.512 760	0.000 008	0.511 802	+4.0	–
6-8b	80.0	16	14.6403	0.827 762	0.000 015	<0.7	9.08	43.27	0.1269	0.512 601	0.000 009	0.511 930	+6.5	787
7-1	47.3	314	0.4362	0.708 155	0.000 010	0.703 134	5.56	23.37	0.1439	0.512 638	0.000 008	0.511 877	+5.5	893
14-11	141	92	4.4576	0.764 279	0.000 014	0.712 968	7.39	40.47	0.1104	0.511 525	0.000 009	0.510 941	−12.9	2244
17-6[b]	128	63.9	5.8405	0.784 470	0.000 022	0.717 240	6.93	34.27	0.1223	0.512 024	0.000 015	0.511 378	−4.3	1695

[a] T_{DM} Nd model ages were calculated after Nelson and DePaolo (1985) for rocks with $^{147}Sm/^{144}Nd < 0.16$.
[b] Data from Kröner et al. (1987); T_{DM} Nd model ages calculated when $^{147}Sm/^{144}Nd < 0.16$

4. Protolith characterisation

We have combined field, petrographical and geochemical data to distinguish between high-grade rocks of igneous (volcanic and/or plutonic) and of sedimentary derivation. Amphibolitic rocks (45–55% SiO_2) are considered as meta-igneous. Gneissic rocks with $SiO_2 > 60\%$ are also considered meta-igneous (orthogneiss) unless their mineral paragenesis is strongly aluminous (i.e. kyanite-, garnet-bearing, or very rich in mica: samples 14-11, 17-6, 7-1, 11-2b). Sample 6-8B (impure quartzite) and sample 6-5 (strongly sodic quartzo-feldspathic gneiss) from Wadi Kurmut are grouped with these paragneisses. Lithological homogeneity of the muscovite–biotite gneisses of El Melagi from western Bayuda suggests a meta-igneous derivation. A similar muscovite gneiss from Khor El Had (sample 14-9) has been grouped with them.

4.1. Meta-igneous rocks

Metabasic rocks (amphibolites) are interlayered with epidote–biotite gneisses and different meta-sedimentary rocks in Khor Dam Et Tor and along Wadi Kurmut (Eastern Bayuda; see Table 1 and Fig. 2 for locations). More homogeneous amphibolite bodies were found at Jebel Absol in eastern Bayuda and in Wadi Umm Tundiba in western Bayuda (Fig. 2).

Metafelsic rocks are subdivided into epidote-bearing and muscovite-bearing biotite gneisses. Epidote-bearing biotite gneisses occur in eastern Bayuda, where they constitute the predominant lithology at Wadi Abu Harik. Biotite and biotite–muscovite gneisses make up large areas in the western Bayuda Desert. At El Melagi (Fig. 2), these granitic orthogneisses are invaded by muscovite-bearing, partly garnetiferous granitic to pegmatitic dykes that are only slightly foliated.

4.2. Meta-sedimentary rocks

Meta-sedimentary rocks comprise garnet–cordierite gneisses, garnet–biotite to garnet–biotite–staurolite–kyanite schists, muscovite schists and some leucocratic gneisses. Other meta-sedimentary lithologies (not sampled) consist of quartzites, graphite schists, calc-silicate-bearing rocks and marbles. In the eastern Bayuda Desert (Wadi Kurmut, Khor Dam Et Tor; Fig. 2), muscovite quartzites, muscovite schists and leucocratic gneisses are intimately associated with orthogneisses; rare kyanite-bearing garnet–biotite–staurolite–schists are found east of Jebel Kurbei. In Khor El Had of the central Bayuda Desert (Fig. 2), garnet–biotite schists without kyanite and staurolite as well as muscovite gneisses occur, straddling the boundary between MVS and GM units. At Sabaloka, garnet–cordierite gneisses occur southeast of Querri station. This granulite facies rock was sampled from the same locality that Kröner et al. (1987) used in their geochronological study.

5. Geochemistry of Bayuda metamorphic rocks

Geochemical data are presented in Table 2.

5.1. Amphibolites

Amphibolites (including garnet and pyroxene-bearing facies) have chemical compositions similar to low-K tholeiitic basalts. A quartz-amphibolite (sample 11-1 from Khor Dam Et Tor) corresponds to a more evolved medium-K calc-alkaline basaltic andesite (Fig. 3A,B).

On chondrite-normalised REE plots, tholeiitic amphibolites, from both eastern (MVS unit) and western Bayuda (GM unit), mostly display patterns with depleted LREE (Fig. 4A, grey zone; $La_N/Yb_N = 0.40–0.94$) and frequent positive Eu anomalies ($Eu/Eu^* = 0.98–1.45$), most likely the effect of plagioclase accumulation during crystallisation. Amphibolites from Khor Dam Et Tor (samples 9-2A and 9-2B; Fig. 4A) show an enhanced positive MREE bulge (Nd–Gd), probably representing accumulation of hornblende. Both features indicate that many amphibolites may not represent liquid compositions (also displayed by the AFM diagram of Fig. 3B). One sample from eastern Bayuda (sample 6-4) and one from western Bayuda (sample 12-6) are particularly low in REE abundance and depleted in LREE (La_N/

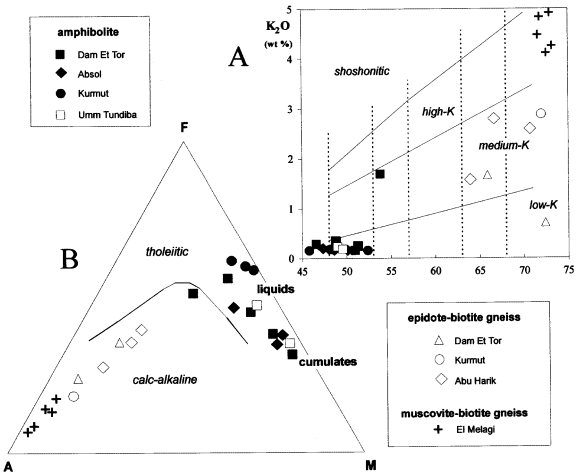

Fig. 3. (A) K_2O versus SiO_2 bivariate diagram. (B) AFM triangular diagram

$Yb_N = 0.06$ and 0.24) and have large positive Eu anomalies (Eu/Eu* = 1.28 and 1.45) but, however, display patterns similar to the main stream. The REE pattern of the calc-alkaline quartz amphibolite (sample 11-1; Fig. 4A) shows a LREE-enriched calc-alkaline-type pattern (La_N/Yb_N = 5.57) with a slightly negative Eu anomaly (Eu/Eu* = 0.89), suggesting incipient plagioclase fractionation.

On MORB-normalised incompatible element plots (Fig. 5A), tholeiitic amphibolites show LILE-enriched and HFSE-depleted patterns characteristic of arc-derived mafic rocks. The rather slight LILE enrichments indicate a primitive island arc or a back-arc environment. Negative and sometimes positive Rb anomalies might be related to increased mobility of this element during high-grade metamorphism. Like for REE, samples 6-4 and 12-6 have lower absolute abundances but rather similar patterns. The normalised patterns of the amphibolites from the western Bayuda Desert are very similar to those from the eastern Bayuda Desert, and suggest formation in a similar palaeo-environment. The quartz-amphibolite from Khor Dam Et Tor (sample 11-1; Fig. 5A) displays higher concentrations in most elements and a stronger Nb–Ta trough characteristic of more evolved island arc magmatism.

In summary, we interpret the amphibolites of Bayuda Desert to represent basaltic volcanism of a primitive evolving to a more mature oceanic convergent margin (oceanic island arc and/or back-arc basin).

5.2. Epidote–biotite and muscovite–biotite orthogneisses

Epidote-bearing biotite orthogneisses from eastern Bayuda have SiO_2 contents between 64 and 73%, and are chemically akin to calc-alkaline low- to medium-K dacites and rhyodacites (Fig. 3A,B). Muscovite-bearing biotite orthogneisses from western Bayuda are potassic with a restricted silica range (72–74% SiO_2) and are classified as high-K calc-alkaline (Fig. 3A,B).

The epidote–biotite orthogneisses are metaluminous to slightly peraluminous and the muscovite–biotite orthogneisses are strongly peraluminous. The latter group has A/CNK values in the range 1.5–2.2 with low $FeO_t + MgO + TiO_2$ (0.6–2.8) values, low CaO/Na_2O (0.2–0.4) ratios, and high Rb/Sr (2–6) and Rb/Ba (0.8–1.6) ratios, characteristic of pelite-derived S-type granites (Sylvester, 1998).

The patterns for the epidote–biotite orthogneisses are only slightly enriched in LREE (Fig. 4B). The medium-K gneisses from Wadi Abu Harik (southeastern Bayuda; La_N/Yb_N = 2.4–4.2) have negative Eu anomalies (Eu/Eu* = 0.74–0.83) and low REE abundance ($\Sigma REE = 40–63$ p.p.m.) for rocks in the 63–71% SiO_2 range. The low-K gneisses from Khor Dam Et Tor (northeastern Bayuda; $La_N/Yb_N = 4.4–4.5$) have positive Eu anomalies (Eu/Eu* = 1.2–1.6) and very low REE abundance ($\Sigma REE = 19–32$ p.p.m.). The contrasting Eu anomalies might be related to plagioclase fractionation for the Abu Harik orthogneisses and hornblende fractionation for the Dam Et Tor orthogneisses. The orthogneiss from Wadi Kurmut is more enriched in LREE (La_N/Yb_N, 21; $\Sigma REE = 72$ p.p.m.) and presents a slight negative Eu anomaly (Eu/Eu* = 0.82).

Representative muscovite–biotite orthogneisses (samples 12-2, 12-3, and 12-5A; Fig. 4C) have fractionated REE spectra ($La_N/Yb_N = 7.8–11.4$),

medium REE abundance ($\Sigma REE = 89–120$ p.p.m.) and large Eu negative anomalies ($Eu/Eu^* = 0.28–0.39$). Sample 12-5B has a lower REE abundance ($\Sigma REE = 38$ p.p.m.) a very weak negative Eu anomaly ($Eu/Eu^* = 0.93$). The Khor El Had sample (14-9) has similar REE abundances and Eu negative anomaly ($\Sigma REE = 66$ p.p.m.; $Eu/Eu^* = 0.31$) but has higher heavy REE (HREE) abundance ($La_N/Yb_N = 4.5$). The garnet-bearing sample (12-1B) has low REE abundance ($\Sigma REE = 29$ p.p.m.) and less large Eu negative anomaly ($Eu/Eu^* = 0.59$), although very low Eu abundance ($Eu = 2.5$ p.p.m.), and, as expected, higher HREE content ($La_N/Yb_N = 4.4$).

On MORB-normalised incompatible element plots (Fig. 5B), the epidote–biotite orthogneisses

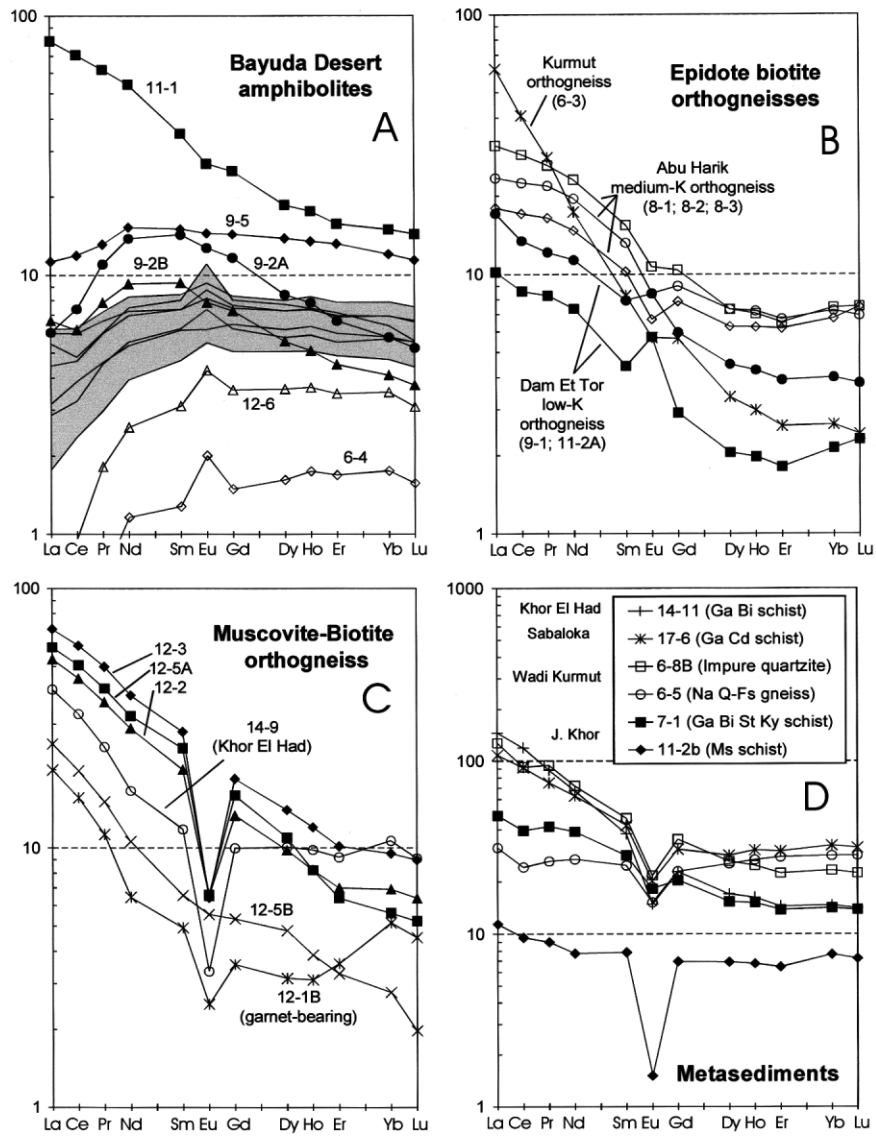

Fig. 4. Chondrite-normalised REE plot (normalising values of Boynton (1984)): (A) amphibolites, grey area enhances the main stream of Bayuda amphibolites; (B) epidote–biotite orthogneisses; (C) muscovite–biotite orthogneisses; and (D) meta-sediments.

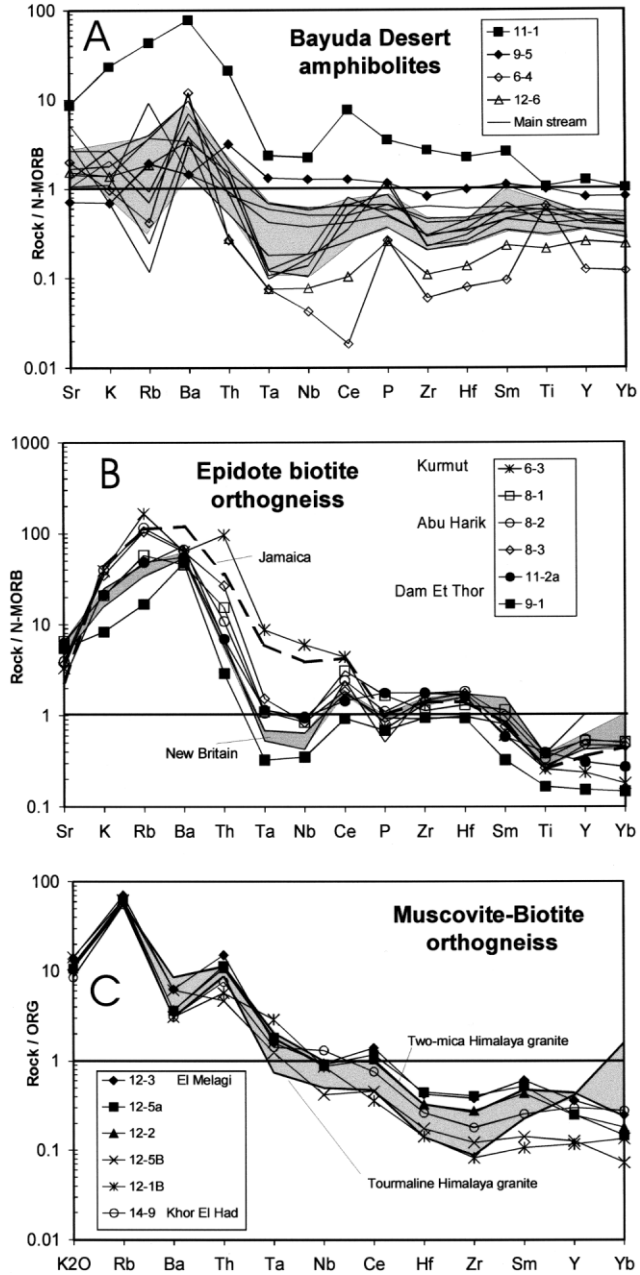

Fig. 5. (A) MORB-normalised spidergram (normalising values of Sun and McDonough (1989)) for amphibolites. Gray field enhances the main stream of Bayuda amphibolites. (B) MORB-normalised spidergram for epidote–biotite orthogneisses; Jamaica and New Britain reference spectra from Pearce et al. (1984), Whalen (1985), respectively. (C) ORG-normalised spidergram (normalising values of Pearce et al. (1984)) for muscovite–biotite orthogneisses. Gray colour enhances the field covered by two Himalayan leucogranites (from Inger and Harris, 1993).

from Dam Et Tor and Abu Harik show the characteristic Nb–Ta trough and Sm, Ti, Y, Yb depletion of subduction-related magmas. The Dam Et Tor low-K gneisses can best be compared with tonalite–granodiorite suites from oceanic island arcs (e.g. New Britain arc, south-western Pacific; Whalen, 1985). The medium-K gneisses from Wadi Abu Harik are slightly more evolved (higher K, Rb and Th) and correspond to more mature arc rocks. Medium-K biotite gneiss from Wadi Kurmut (sample 6-3) shows positive anomalies for Rb and Th that are typical of crustally contaminated continental margin arc magmas. However, the abundances of Rb, Th, Ba are similar to some uncontaminated magmas from oceanic subduction settings (e.g. Jamaica; Pearce et al., 1984).

On ORG-normalised incompatible element plots (Fig. 5C), the muscovite–biotite orthogneisses from El Melagi and Khor El Had are characterised by a positive Rb peak and only a slight Nb–Ta negative anomaly. Spectra of enriched El Melagi samples (12-3, 12-5A, 12-2) and Khor El Had orthogneiss (14-9) are very similar to syn-collisional 2-mica peraluminous granites from Himalaya (Inger and Harris, 1993). Samples with lower concentrations (samples 12-5B and 12-1B) have subparallel spectra closer to the Himalaya tourmaline-bearing granite (Inger and Harris, 1993), except for HREE where only a slight enrichment is shown by sample 12-1B.

In conclusion, we can interpret the epidote-bearing orthogneisses from Khor Dam Et Tor and Wadi Abu Harik to represent felsic volcanism in an oceanic arc environment, and the muscovite–biotite orthogneisses from Melagi and Khor El Had as syn-collisional peraluminous intrusive granitoids.

5.3. Meta-sediments

Most of the paragneisses and schists are fairly siliceous (SiO_2 contents between 70 and 80%), except the kyanite- and staurolite-bearing schists from Jebel Kurbei (sample 6-1, 64% SiO_2). Ga–Bi (14-11) and Ga–Cd (17-6) schists are richer in iron (5–6%) than average igneous rocks for such a silica content (71%); they have low Na_2O and high K_2O content when compared with the epidote–biotite orthogneisses, resulting probably from an ancient weathering. This is also the case for the quartz–feldspar gneiss (sample 6-5), nearly devoid of K_2O (0.17%) and for the impure quartzite (sample 6-8B), nearly devoid of Na_2O (0.1%).

In geochemical classification diagrams for terrigeneous sediments (e.g. the classification of Herron (1988); data not shown), most of the schists and gneisses classify as arkoses and graywackes. The kyanite- and staurolite-bearing garnet–biotite schist (sample 7-1) plots as shale, while the sodic quartz–feldspar gneiss (sample 6-5) is classified as Fe-sand.

Three meta-sedimentary rocks (samples 14-11, 17-6 and 6-8B) have LREE-enriched patterns ($\Sigma REE = 220–505$ p.p.m.; La_N/Yb_N, 3.4–10.3), while the three others (samples 6-5, 7-1 and 11-2B) have flatter and lower patterns ($\Sigma REE = 26–100$ p.p.m.; La_N/Yb_N, 1.1–3.5) (Fig. 4D). An interesting feature of the latter is their negative Ce anomaly. Such an anomaly is characteristic for river and seawater, and could be obtained by prolonged subaquatic weathering. However, it could also indicate an island arc or a back arc source where this kind of anomaly is known (Shimizu et al., 1992; Gribble et al., 1998); the latter interpretation agrees also with their positive ε_{Nd} values (see later).

These few REE patterns suggest, then, an island arc volcanogenic source for eastern Bayuda schists and a more continental source for Sabaloka and western Bayuda ones.

6. Geochronology and isotope geochemistry

6.1. Sm–Nd whole rock dating and Nd initial isotopic ratios

Age calculations have been made following Ludwig (1999), all errors being given at the 2σ level.

The eight analysed amphibolites define an isochron of 810 ± 32 Ma (Nd initial ratio (NdIR) $= 0.511\,858 \pm 40$, equivalent to $\varepsilon_{Nd\text{-}810} = +5.2 \pm 0.8$, MSWD $= 0.47$; Fig. 6A). The three analysed epidote–biotite gneisses, also representing metavolcanic rocks, fall on the same isochron

giving (Fig. 6A) 806 ± 19 Ma, NdIR = $0.511\,865 \pm 20$ ($\varepsilon_{Nd} = +5.2 \pm 0.4$), MSWD = 1.4 for 11 WR. These ages and NdIR are very similar. As such homogeneous Nd initial ratios cannot be produced by metamorphism, particularly on the large area covered by these samples (Fig. 2B), we interpret the age of 806 ± 19 Ma as the emplacement of the arc magmas and the ε_{Nd} value of $+5.2 \pm 0.4$ as representing that of the mantle magma source.

Meta-sediments have variable Nd isotope ratios, some lying close to the metavolcanic isochron, others largely below it (Fig. 6B). They yield ε_{Nd} values at 806 Ma varying from $+6$, a value close to that of the arc magmas, down to -13 (Table 3). This indicates that the meta-sedi-

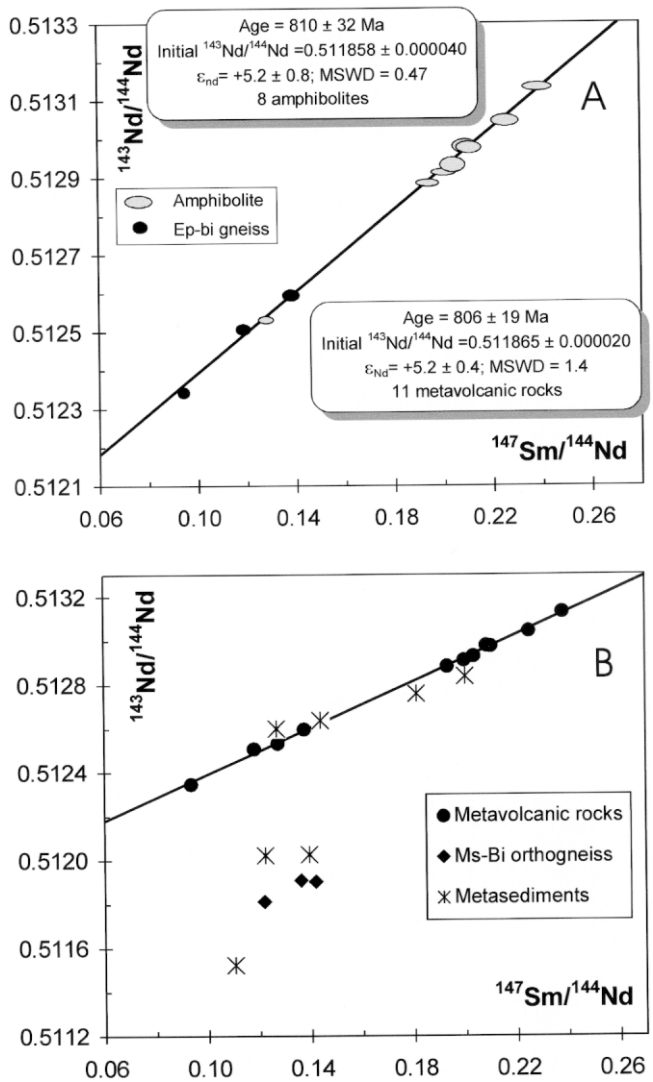

Fig. 6. (A) Sm–Nd isochrons for the eight amphibolites and for 11 metavolcanic rocks (eight amphibolites + three epidote–biotite gneisses). (B) Position of the meta-sediments and of the muscovite–biotite peraluminous orthogneiss relatively to the metavolcanic rock isochron.

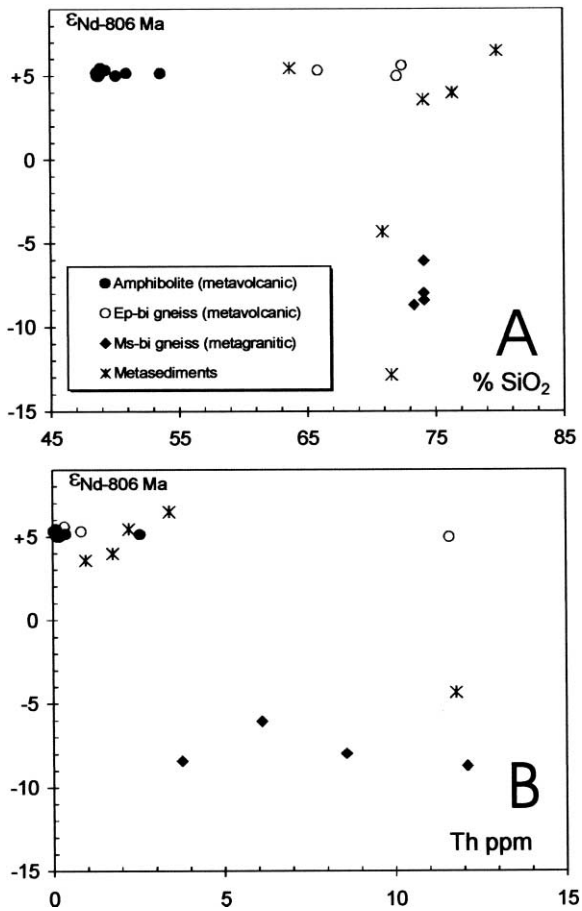

Fig. 7. ε_{Nd} value at 806 Ma for metamorphic rocks from Bayuda Desert versus SiO_2 (A) and Th p.p.m. (B). (Isotopic data for Sabaloka meta-sedimentary gneiss are from Kröner et al. (1987).) Muscovite–biotite orthogneiss could be younger than 806 Ma, perhaps as young as 700 Ma, but this does not change a lot the position of the samples.

ments represent material coming exclusively from the oceanic island arc (Eastern Bayuda) as well as material from an older continental mass (western Bayuda and Sabaloka).

The muscovite–biotite orthogneisses, representing metamorphosed S-type granites, are located well below the isochron of the metavolcanic rocks (Fig. 6B), giving ε_{Nd} values between -8 and -9 at 806 Ma. These ε_{Nd} values are in the range of the meta-sediments containing old material.

The ε_{Nd} values are not correlated with SiO_2 contents (Fig. 7A). Negative ε_{Nd} values are not linked to an AFC process and felsic rocks of mantle origin have been generated. Several meta-sediments are silica-rich and in the range of the Bayuda island arc/back arc rocks. Except one, the island arc rocks and derived sediments are Th poor; even the felsic ones, by opposition to the samples having an old continental crust signature (Fig. 7B). Sample 6-3, with 12 p.p.m. Th, could indicate that the Bayuda island arc became quite thick, allowing Th enrichment as proposed for the 2 Ga old Birimian island arc (Ama Salah et al., 1996).

6.2. Rb–Sr whole rock dating and Sr initial ratios

The very low Rb content and Rb/Sr ratios of the metavolcanic rocks (Table 3) do not allow calculation of confident isochrons. Nine metavolcanic rocks (without the two Umm Tundiba amphibolites; see later) give an errorchron (MSWD = 3.3) of 616 ± 120 Ma (SrIR = $0.703\,56 \pm 0.000\,54$; data not shown) that is mainly controlled by sample 6-3, with a much larger Rb/Sr ratio (Table 3). This imprecise age suggests that the Rb–Sr isotopic system was affected by late Pan-African metamorphism. Whether this mobility is related to the collisional event at approximately 700 Ma or the younger HT metamorphism at approximately 600 Ma is difficult to resolve. Recent work on granulites from Sabaloka has yielded concordant U–Pb monazite ages of 622 Ma (V. Schenk, personal communication) that may be interpreted as the beginning of final uplift and crustal cooling at Sabaloka. This event may also have occurred at Bayuda.

As the radiogenic growth of Sr is very small in these metavolcanic rocks due to low Rb/Sr ratios, precise Sr initial ratios can be calculated. With the exception again of the two Umm Tundiba amphibolites, the Sr initial ratios at 806 Ma of the Bayuda metavolcanic rocks are low, with a mean value of 0.7033 ± 0.0006 (9 WR). This mean Sr initial ratio is consistent with the mean ε_{Nd} value of $+5.2 \pm 0.4$, in agreement with a depleted mantle island arc source.

The higher initial Sr isotopic ratios of the two Umm Tundiba amphibolites at approximately 0.708, close to the measured values (Table 3), for a ε_{Nd} value of approximately $+5$ can be ascribed

to a younger Sr disturbance, as Nd isotopes indicate the same age and source (Fig. 6A). As these amphibolites are spatially associated with the El Melagi S-type granitoid gneisses, their high Sr initial ratios could be the result of radiogenic ^{87}Sr uptake. The granitoid gneisses are Rb-rich and will consequently acquire rapidly a high content in radiogenic ^{87}Sr, easily mobilised during metamorphism.

The meta-sediments have variable Sr initial ratios at 806 Ma (0.695–0.720). The two samples with low Rb/Sr ratios (samples 6-5 and 7-1) have a SrIR close to that of the metavolcanic rocks (0.7038 and 0.7032), in agreement with their ε_{Nd} values of $+4.0$ and $+5.5$, respectively. The other samples have high $^{87}Rb/^{86}Sr$ ratios (from 1.5 to 14) and give dispersed SrIR, sometimes <0.7 (Table 3). This again indicates Sr isotope mobility during a later metamorphic event. No reliable Rb–Sr ages can be calculated with these rocks.

6.3. T_{DM} Nd model ages

Mafic metavolcanic rocks have generally Sm/Nd ratios close to mantle values that preclude the calculation of significant T_{DM} Nd model ages (sample and depleted mantle Nd evolution are subparallel and do not determine meaningful intersections). Only samples having $^{147}Sm/^{144}Nd$ ratios <0.16 have been considered for T_{DM} calculations (Table 3; calculated following Nelson and DePaolo, 1985).

This is the case of the quartz amphibolite (sample 11-1) that gave a T_{DM} Nd model age of 903 Ma. T_{DM} Nd model ages of the epidote–biotite gneisses (felsic metavolcanic rocks) from eastern Bayuda are around 900 Ma (Table 3), only slightly older than their emplacement age, as for the quartz amphibolite. T_{DM} Nd model ages so close to emplacement ages indicate virtually no contribution of older continental crust in the genesis of these felsic rocks.

The T_{DM} Nd model ages of the meta-sedimentary rocks vary between 0.79 and 2.42 Ga (Table 3). Neoproterozoic T_{DM} ages of the volcanogenic meta-sediments from eastern Bayuda indicate the contemporaneous magmatic arc as the primary source of the sediments. The meta-sedimentary rock from Khor El Had in central Bayuda and the muscovite–biotite granitoid gneisses from western Bayuda have Palaeoproterozoic T_{DM} Nd model ages (2.06–2.42 Ga). The granulite facies terrigeneous meta-sediment from Sabaloka (isotope data from Kröner et al., 1987) has a Mesoproterozoic T_{DM} age of 1.69 Ga, similar to the 1.58 and 1.63 Ga T_{DM} ages reported by Harris et al. (1984) for meta-sedimentary gneisses from the Rahaba mine area of central Bayuda. This either means denudation of isotopically heterogeneous continental crust in the source region or mixing of different sources during or at the site of deposition. The Mesoproterozoic T_{DM} Nd model ages are probably best explained by mixing of detritus from Palaeoproterozoic and Neoproterozoic sources that were shed into the basin at the same time.

7. Pan-African geodynamic scenario for the Bayuda Desert and regional implications

The Neoproterozoic oceanic island arc/back arc signature of the metavolcanic rocks from Bayuda Desert precludes the interpretations invoquing two oceanic re-entrants within an old Bayuda terrane (Abdelsalam et al., 1998) or considering that the Halfa and Bayuda terranes were initially one old block, separated by a small-sized oceanic basin (Delgo suture) and reunited afterwards (Schandelmeier et al., 1994). A more mobilistic model has to be set up.

In addition to the granitoid orthogneisses, two key lithological elements are apparent in the Bayuda Desert: arc-related volcanic and sedimentary rocks, and continent-derived terrigeneous sediments. It is unclear whether the two associations are laterally linked in time and space or whether they represent a stratigraphic or structural succession. They could be interfingered (Barth and Meinhold, 1979). This implies that the Bayuda Desert corresponds to a Pan-African back-arc basin bordered by an intra-oceanic island arc to the east and, at a given time, by an older continent to the west. This system was initially active at 806 ± 19 Ma, producing primitive tholeiitic to moderately evolved calc-alkaline magmas, with derivative sediments probably as a

volcaniclastic apron. At an unknown time but before 700 Ma (collision between the Bayuda and Halfa terranes; Harms et al., 1994), continental debris were transported from the western sides into the basin, indicating the proximity of a continent and probably the imminence of the collision. Indeed, the juvenile Neoproterozoic isotope characteristics of the Wadi Kurmut biotite gneiss (sample 6-3) favour an oceanic crustal floor for the back-arc basin. This gneiss has a mature arc geochemical signature but its isotopic composition indicates that pre-Neoproterozoic crust was not present during the evolved stage of arc development.

Collision with the Halfa terrane to the north occurred before approximately 700 Ma (Harms et al., 1994). Obduction of the Delgo ophiolite to the SE onto the Bayuda terrane indicates a subduction zone likely dipping to the NW, beneath the Halfa terrane. The subduction zone that produced the Bayuda island arc was situated on the eastern side of the Bayuda terrane, and most likely had a rather similar dip towards the west or northwest. During collision, slivers of oceanic material became stacked together with the terrigeneous metasediments, the moment when the peraluminous El Melagi-type granite probably intruded.

What occurred afterwards is poorly recorded in the Bayuda desert except that the Rb–Sr isotopic system was disturbed probably at around 600 Ma or did not close before 600 Ma. Just to the east, the Keraf suture zone functioned as a sinistral transpression mega-shear zone between 640 and 580 Ma (Abdelsalam et al., 1998). Such a structure active for 60 Ma can account for an approximately 1000 km relative movement (with a mean rate of 1–2 cm of movement per year; Jarrard, 1986), here between the Gerf–Gabgaba–Gebeit terranes and the Bayuda–Halfa terranes (Fig. 2). This is a typical post-collisional environment (Liégeois, 1998), associated with abundant high-K calc-alkaline and late alkaline granitoids (Küster and Harms, 1998). Such late and large movements render very difficult a palaeogeographical reconstruction prior to 640 Ma. For example, convergence of the Gabgaba–Gebeit terrane was also well under way before 700 Ma (Bailo, 2000), but not necessarily with the Bayuda terrane, their juxtaposition resulting from the late horizontal work of the Keraf shear zone.

The Keraf zone, however, represents a major plate boundary as it separates not only terranes with different Pan-African metamorphic facies (greenschist to the east and amphibolitic-granulitic to the west), but also different mantle sources. Indeed, if arc-related volcanic activity in the Bayuda Desert (approximately 800 Ma) is largely coeval with 852–735 Ma old arc volcanism in the Gabgaba–Gebeit terrane of the ANS, its source characteristics are discernibly different, giving rise to higher T_{DM} Nd model ages (around 900 Ma for 750–800 Ma). This is due to the fact that the isotopic composition of the mantle source of the Bayuda metavolcanic rocks is less depleted (ε_{Nd}, $+5.2 \pm 0.4$) than the source of the Gabgaba–Gebeit metavolcanic rocks (ε_{Nd}, $+6.5$ to $+8.4$; Stern and Kröner, 1991; Reischmann and Kröner, 1994; Stern and Abdelsalam, 1998). As the Bayuda felsic arc-related rocks have similar ε_{Nd} values, around $+5$, as the metabasalts, this cannot be attributed to an old continental crust contamination. A similar conclusion has been reached for the Moya charnockites and enderbites (ε_{Nd} approximately $+3$ at 740 Ma; Stern and Dawoud, 1991) (see Fig. 2 for location) that could belong to the same lithospheric entity as Bayuda. However, less depleted mantle sources of early Pan-African (>800 Ma) subduction-related magmatism are also reported from the ANS itself. Rocks from Haya terrane, southern Red Sea Hills of Sudan (Kröner et al., 1991), and from the Axum area of northern Ethiopia (Tadesse et al., 2000) have similar ε_{Nd} values between $+3$ and $+6$. The significance of these data, i.e. whether or not all of these areas belonged to the same lithospheric entity, has yet to be determined.

Orthogneisses from Wadi Abu Harik in the southeasternmost Bayuda Desert (just west of Atbara; Fig. 2) have ε_{Nd} values of $+7.0$ (Harris et al., 1984) and, if the isotopic correlations are correct, would not belong to the Bayuda terrane. Barth and Meinhold (1979) mapped this part of the Bayuda Desert as the distinct Abu Harik Formation (5% of the Bayuda surface). They suggested a tectonic contact or a discontinuity between the two formations. The Abu Harik

Formation would then belong to the Keraf zone, itself included into the Gabgaba–Gebeit terrane assembly.

West of the Keraf suture, the trending structures are dominantly NE–SW until the Uweinat Archaean nucleus and concern large areas of high-grade metamorphic rocks. Geological knowledge of this huge area is still very low. However, high-grade meta-sediments (micaschists, quartzofeldspathic gneisses, quartzites and graphite schists) and metavolcanic rocks (amphibolites) make up significant portions of the lithologies in these areas (Wahab and Afia 1966; Babiker, 1971; Vail, 1972; Schandelmeier and Richter, 1991; Lattard et al., 1993). It therefore seems possible that a former Pan-African oceanic convergent domain extends into western Sudan. Between the Bayuda Desert and the Archaean nucleus of Uweinat, isolated outcrops of basement in northwestern Sudan and southwestern Egypt (see Figs. 1 and 2) are mainly composed of granitic to tonalitic gneisses and migmatites. They are interpreted as the products of Pan-African remelting of Palaeoproterozoic crust (Harms et al., 1990; Sultan et al., 1994). Similar gneisses are found as lower crustal xenoliths in Cenozoic lavas of Jebel Marra volcano in western Sudan (Davidson and Wilson, 1989).

We then propose as a hypothesis that this large oceanic domain accreted with the East Saharan ghost craton, here identified in the Uweinat area, during an intense NW-directed frontal collision (in fact probably a series of collisions) at approximately 700 Ma. It induced the regional amphibolite–granulite facies metamorphism into the juvenile terranes and the re-melting of older terranes to the NW. The terranes from the Arabian–Nubian shield arrived in the same age range, but through a more oblique and softer collision continuing with horizontal displacements along mega-shear zones, inducing only greenschist facies metamorphism.

This indicates that the East Saharan ghost craton probably lies east of the Zalingei zone (Vail, 1972, 1976; Fig. 2), although it cannot be excluded that some parts of the juvenile terranes, could be thrust upon the ESGC, which could then be present at depth.

Whether or not this cratonic area extends further to the west and connects with the other cratonic area evidenced east of the Tuareg shield (Liégeois et al., 1994, 2000; Fig. 1) is not yet possible to assess; in particular, whether a decratonisation process occurred during the Pan-African in this lithospheric domain (Black and Liégeois, 1993).

8. Conclusions

The Bayuda Desert basement is not, as previously thought, a part of a pre-Neoproterozoic 'East Saharan Craton'. Instead, it is made up of Neoproterozoic (806 ± 19 Ma) metavolcanic rocks and meta-sediments that were formed in an island arc/marginal basin setting. The associated sediments were derived from an oceanic arc, some of them mixed with a pre-Neoproterozoic continental source.

Amphibolite facies high-grade metamorphism and peraluminous granites in Bayuda Desert are related to a major frontal collision between the Bayuda and Halfa terranes at approximately 700 Ma (Harms et al., 1994) probably within the framework of a composite collision with the East Saharan ghost craton, represented to the NW by the Uweinat Archaean nucleus.

The oblique collision that affected the Gabgaba–Gebeit terrane was initiated in the same age range (before 700 Ma) but perhaps not with the Bayuda terrane. Their juxtaposition occurred later (640–580 Ma) through a large sinistral transpressive displacement along the Keraf mega-shear zone (Abdelsalam et al., 1998). In Bayuda, this event resulted in disturbance of Rb–Sr isotope systematics and intrusion of granites. This later phase is typically post-collisional (Liégeois, 1998).

Large areas in central and western Sudan share lithological and structural similarities with the Bayuda Desert basement. It is thus proposed that a Pan-African oceanic convergent margin association extends further to the west. This argues for a mobilistic interpretation of the Pan-African orogen north of the Congo Craton. The areas between the Zalingei zone (inclusive) and the Keraf zone (exclusive), and possibly beyond its southern

prolongation (Fig. 2), seem to share lithological and structural similarities: most important are a common oceanic convergent margin environment (800–720 Ma) and an early Pan-African frontal collision (approximately 700 Ma) with the East Saharan ghost craton inducing high-grade metamorphism. This large area does not belong to the East Saharan ghost craton. However, since some of these allochtonous terranes could have been thrust upon it during the Pan-African frontal collision, it cannot be precluded that cratonic material is present at depth.

Acknowledgements

The authors would like to thank Ahmed S. Dawoud and his coworkers for guidance and assistance in the field, and Gerhard Franz for commenting on an earlier version of the manuscript. The first author appreciates the financial support of Deutsche Forschungsgemeinschaft (grant Ku-887/3-1). We thank Bob Stern and Stefan Jung for their detailed and constructive reviews that encouraged us to prune off dead branches to strengthen the manuscript.

References

Abdel Rahman, E.M., 1993. Geochemical and geotectonic controls of the metallogenetic evolution of selected ophiolite complexes from the Sudan. Berliner Geowiss. Abh. A145, 175.

Abdel Rahman, E.M., Harms, U., Schandelmeier, H., Franz, G., Darbyshire, D.P.F., Horn, P., Müller-Sohnius, D., 1991. A new ophiolite occurrence in NW Sudan — constraints on Late Proterozoic tectonism. Terra Nova 2, 363–376.

Abdelsalam, M.G., Stern, R.J., 1996. Sutures and shear zones in the Arabian–Nubian Shield. J. Afr. Earth Sci. 23, 289–310.

Abdelsalam, M.G., Stern, R.J., Schandelmeier, H., Sultan, M., 1995. Deformational history of the Neoproterozoic Keraf Zone in NE Sudan, revealed by shuttle imaging radar. J. Geol. 103, 475–491.

Abdelsalam, M.G., Stern, R.J., Copeland, P., Elfaki, E.M., Elhur, B., Ibrahim, F.M., 1998. The Neoproterozoic Keraf Suture in NE Sudan: sinistral transpression along the eastern margin of West Gondwana. J. Geol. 106, 133–148.

Almond, D.C., 1980. Precambrian events at Sabaloka, near Khartoum, and their significance in the chronology of the basement complex of North-East Africa. Precambr. Res. 13, 43–62.

Ama Salah, I., Liégeois, J.P., Pouclet, A., 1996. Evolution d'un arc insulaire océanique birimien précoce au Liptako nogérien (Sirba): géologie, géochronologie et géochimie. J. Afr. Earth Sci 22, 235–254.

Babiker, I.M., 1971. Geology of sheet Tagabo Hills (no. 54-F). Geology Survey Department Memoir 4. Geological Survey Department of the Sudan, Khartoum, 37 pp.

Bailo, T., 2000. Keraf Shear Zone, NE Sudan: geodynamic characteristics of the Nile Craton–Nubian Shield boundary. Unpublished Ph.D. Thesis. Technical University of Berlin, 138 pp.

Barth, H., Meinhold, K.D., 1979. Mineral prospecting in the Bayuda Desert. Unpublished Technical Report of the Sudanese–German Exploration Project, Vol. A. BGR, Hannover, 336 pp.

Black, R., Liégeois, J.P., 1993. Cratons, mobile belts, alkaline rocks and the continental lithospheric mantle: the Pan-African testimony. J. Geol. Soc. Lond. 150, 89–98.

Black, R., Latouche, L., Liégeois, J.P., Caby, R., Bertrand, J.M., 1994. Pan-African displaced terranes in the Tuareg shield (central Sahara). Geology 22, 641–644.

Boynton, W.V., 1984. Geochemistry of the rare earth elements: meteorite studies. In: Henderson, P. (Ed.), Rare Earth Element Geochemistry. Elsevier, Amsterdam, pp. 63–114.

Davidson, J.P., Wilson, I.R., 1989. Evolution of an alkali basalt-trachyte suite from Jebel Marra volcano, Sudan, through assimilation and fractional crystallization. Earth Planet. Sci. Lett. 95, 141–160.

Denkler, T., Franz, G., Schandelmeier, H., 1994. Tectonometamorphic evolution of the Neoproterozoic Delgo sture zone, Northern Sudan. Geol. Rundschau 83, 578–590.

El Rabaa, S.M., 1976. Structural and metamorphic evolution of west Berber district, Sudan, with special reference to the structural control of mica-bearing pegmatites. In: Tsegaye, H. (Ed.), Proceedings of the 2nd Conference on African Geology, Addis Abeba, 1973, pp 81–96, Geology Society of Africa.

Greiling, R.O., Abdeen, M.M., Dardir, A.A., El Akhal, H., El Ramly, M.F., Kamal El Din, G.M., Osman, A.F., Rashwan, A.A., Rice, A.H.N., Sadak, M.F., 1994. A structural synthesis of the Proterozoic Arabian–Nubian shield in Egypt. Geol. Rundschau 83, 484–501.

Gribble, R.F., Stern, R.J., Newman, S., Bloomer, S.H., O'Hearn, T., 1998. Chemical and isotopic composition of lavas from the Northern Mariana trough: implications for magma genesis in back-arc basins. J. Petrol. 39, 125–154.

Harms, U., Schandelmeier, H., Darbyshire, D.P.F., 1990. Pan-African reworked early/middle Proterozoic crust in NE Africa west of the Nile: Sr and Nd isotope evidence. J. Geol. Soc. Lond. 147, 859–872.

Harms, U., Darbyshire, D.P.F., Denkler, T., Hengst, M., Schandelmeier, H., 1994. Evolution of the Neoproterozoic Delgo suture zone and crustal growth in northern Sudan: geochemical and radiogenic isotope constraints. Geol. Rundschau 83, 591–603.

Harris, N.B.W., Hawkesworth, C.J., Ries, A.C., 1984. Crustal evolution in north-east and East Africa from model Nd ages. Nature 309, 773–776.

Herron, M.M., 1988. Geochemical classification of terrigenous sands and shales from core or log data. J. Sediment. Petrol. 58, 820–829.

Inger, S., Harris, N.B.W., 1993. Geochemical constraints on leucogranite magmatism in the Langtang valley, Nepal Himalaya. J. Petrol. 34, 345–368.

Jarrard, R.D., 1986. Terrane motion by strike-slip faulting of forearc slivers. Geology 14, 780–783.

Klerkx, J., Deutsch, S., 1977. Résultats préliminaires obtenus par la méthode Rb/Sr sur l'âge des formations précambriennes de la région d'Uweinat (Libye). Musée R. Afr. Centrale Dépt. Géol. Min. Rapp. Ann. 1976, 83–94.

Kröner, A., 1979. Pan-African plate tectonics and its repercussions on the crust of northeast Africa. Geol. Rundschau 68, 565–583.

Kröner, A., Stern, R.J., Dawoud, A.S., Compston, W., Reischmann, T., 1987. The Pan-African continental margin in northeastern Africa: evidence from a geochronological study of granulites at Sabaloka, Sudan. Earth Planet. Sci. Lett. 85, 91–104.

Kröner, A., Linnebacher, P., Stern, R.J., Reischmann, T., Manton, W., Hussein, I.M., 1991. Evolution of Pan-African island arc assemblages in the southern Red Sea Hills, Sudan, and in southwestern Arabia as exemplified by geochemistry and geochronology. Precambr. Res. 53, 99–118.

Küster, D., 1995. Rb–Sr isotope systematics of muscovite from Pan-African granitic pegmatites of Western and Northeastern Africa. Mineral. Petrol. 55, 71–83.

Küster, D., Harms, U., 1998. Post-collisional potassic granitoids from the southern and northwestern parts of the Late Neoproterozoic East African Orogen: a review. Lithos 45, 177–195.

Lattard, D., von Goerne, G., Franz, G., 1993. Metamorphic evolution of the Pan-African basement in the Meidob volcanic field (Darfur Dome, Sudan). In: Thorweihe, U., Schandelmeier, H. (Eds.), Geoscientific research in northeast Africa. Balkema, Rotterdam, pp. 161–163.

Liégeois, J.P., 1998. Some words on the post-collisional magmatism. Lithos 45, xv–xviii.

Liégeois, J.P., Black, R., Navez, J., Latouche, L., 1994. Early and late Pan-African orogenies in the Aïr assembly of terranes (Tuareg shield, Niger). Precambrian Res. 67, 59–88.

Liégeois, J.P., Latouche, L., Navez, J., Black, R., 2000. Pan-African collision, collapse and escape tectonics in the Tuareg shield: relations with the East Saharan Ghost craton and the West African craton. 18th Colloquium of African Geology, Graz, Austria [abstract]. J. Afr. Earth Sci 30, 53–54.

Ludwig, K.R., 1999, Using Isoplot/Ex Version 2.01, A Geochronological Toolkit for Microsoft Excel. Berkeley Geochronology Center Special Publication No. 1a, Berkeley, CA, 47 pp.

Meinhold, K.D., 1979. The Precambrian basement complex of the Bayuda Desert, northern Sudan. Rev. Géol. Dyn. Géogr. Phys. 21, 395–401.

Nelson, B.K., DePaolo, D.J., 1985. Rapid production of continental crust 1.7 to 1.9 b.y. ago: Nd isotopic evidence from the basement of the North Americam midcontinent. Geol. Soc. Am. Bull. 96, 746–754.

Pearce, J.A., Harris, N.B.W., Tindle, A.G., 1984. Trace element discrimination diagrams for the tectonic interpretation of granitic rocks. J. Petrol. 25, 956–983.

Pin, C., Poidevin, J.L., 1987. U–Pb zircon evidence for a Pan-African granulite facies metamorphism in the Central African Republic. A new interpretation of the high-grade series of the northern border of the Congo craton. Precambr. Res. 36, 303–312.

Pinna, P., Calvez, J.Y., Abessolo, A., Angel, J.M., Mekoulou-Mekoulou, T., Mananga, G., Vernhet, Y., 1994. Neoproterozoic events in the Tcholliré area: Pan-African crustal growth and geodynamics in central-northern Cameroon (Adamawa and North Provinces). J. Afr. Earth Sci. 18, 347–353.

Reischmann, T., Kröner, A., 1994. Late Proterozoic island arc volcanics from Gebeit, Red Sea Hills, north-east Sudan. Geol. Rundschau 83, 547–563.

Ries, A.C., Shackleton, R.M., Dawoud, A.S., 1985. Geochronology, geochemistry and tectonics of the NE Bayuda Desert N Sudan: implication for the western margin of the late Proterozoic fold belt of NE Africa. Precambr. Res. 30, 43–62.

Rogers, J.J.W., Ghuma, M.A., Nagy, R.M., Greenberg, J.K., Fullagar, P.D., 1978. Plutonism in Pan-African belts and the geologic evolution of notheastern Africa. Earth Planet. Sci. Lett. 39, 109–117.

Schandelmeier, H., Richter, A., 1991. Brittle shear deformation in Northern Kordofan, Sudan: late Carboniferous to Triassic reactivation of Precambrian fault systems. J. Struct. Geol. 13, 711–720.

Schandelmeier, H., Richter, A., Harms, U., 1987. Proterozoic deformation of the East Sahara Craton in southeast Libya, south Egypt and north Sudan. Tectonophysics 140, 233–246.

Schandelmeier, H., Utke, A., Harms, U., Küster, D., 1990. A review of the Pan-African evolution of NE Africa: towards a new dynamic concept for continental NE Africa. Berliner Geowiss. Abh. A120, 1–14.

Schandelmeier, H., Wipfler, E., Küster, D., Sultan, M., Becker, R., Stern, R.J., Abdelsalam, M.G., 1994. Atmur-Delgo suture: a Neoproterozoic oceanic basin extending into the interior of northeast Africa. Geology 22, 563–566.

Shimizu, H., Sawatari, H., Kawata, Y., Dunkley, P.N., Masuda, A., 1992. Ce and Nd isotope geochemistry on island

arc volcanic rocks with negative Ce anomaly: existence of sources with concave REE patterns in the mantle beneath the Solomon and Bonin island arcs. Contrib. Mineral. Petrol. 110, 242–252.

Stern, R.J., 1994. Neoproterozoic (900–550 Ma) arc assembly and continental collision in the East African Orogen: implications for the consolidation of Gondwanaland. Annu. Rev. Earth Planet. Sci. 22, 319–351.

Stern, R.J., Abdelsalam, M.G., 1998. Formation of juvenile continental crust in the Arabian–Nubian shield: evidence from granitic rocks of the Nakasib suture, NE Sudan. Geol. Rundschau 87, 150–160.

Stern, R.J., Dawoud, A.S., 1991. Late Precambrian (740 Ma) charnockite, enderbite, and granite from Jebel Moya, Sudan: a link between the Mozambique Belt and the Arabian-Nubian Shield? J. Geol. 99, 648–659.

Stern, R.J., Kröner, A., 1991. Late Precambrian crustal evolution in NE Sudan: isotopic and geochronological constraints. J. Geol. 101, 555–574.

Stern, R.J., Abdelsalam, M.G., Schandelmeier, H., Sultan, M., Wickham, S., 1993. Carbonates of the Keraf Zone, NE Sudan: a Neoproterozoic (ca. 750 Ma) passive margin on the eastern flank of west Gondwanaland? Geol. Soc. Am. 27, 49 (abstract with Programme).

Stern, R.J., Kröner, A., Bender, R., Reischmann, T., Dawoud, A.S., 1994. Precambrian basement around Wadi Halfa, Sudan: a new perspective on the evolution of the East Saharan Craton. Geol. Rundschau 83, 564–577.

Sultan, M., Tucker, R.D., El Alfy, Z., Attia, R., Ragab, A.G., 1994. U–Pb (zircon) ages for the gneissic terrane west of the Nile, southern Egypt. Geol. Rundschau 83, 514–522.

Sun, S.S., McDonough, W.F., 1989. Chemical and isotope systematics of oceanic basalts: implications for mantle composition and processes. In: Saunders, A.D., Norry, M.J. (Eds.), Magmatism in Ocean Basins. Geology Society of London Special Publication, vol. 42. Geology Society of London, London, pp. 313–345.

Sylvester, P.J., 1998. Post-collisional strongly peraluminous granites. Lithos 45, 29–44.

Tadesse, T., Hoshino, M., Suzuki, K., Izumi, S., 2000. Sm–Nd, Rb–Sr and Th–U–Pb zircon ages of syn- and post-tectonic granitoids from the Axum area of northern Ethiopia. J. Afr. Earth Sci. 30, 313–327.

Toteu, S.F., Macaudiere, J., Bertrand, J.M., Dautel, D., 1990. Metamorphic zircons from North Cameroon: implications for the Pan-African evolution of Central Africa. Geol. Rundschau 79, 777–788.

Vail, J.R., 1971. Geological reconnaissance in part of Berber District, Northern Province, Sudanese Geology Survey Department Bulletin 18. Geological Survey Department of the Sudan, Khartoum, 76 pp.

Vail, J.R., 1972. Geological reconnaissance in the Zalingei and Jebel Marra areas of western Darfur Province. Sudanese Geology Survey Department Bulletin 14. Geological Survey Department of the Sudan, Khartoum, 50 pp.

Vail, J.R., 1976. Outline of the geochronology and tectonic units of the basement complex of Northeast Africa. Proc. R. Soc. Lond. Ser. A 350, 127–141.

Vail, J.R., 1979. Outline of geology and mineralization of the Nubian Shield east of the Nile Valley, Sudan. In: Tahon, S.A. (Ed.), Evolution and Mineralization of theArabian–Nubian Shield, vol. 1:. Pergamon Press, Oxford.

Vail, J.R., 1988. Tectonics and evolution of the Proterozoic basement of Northeastern Africa. In: El-Gaby, S., Greiling, R. (Eds.), The Pan-African Belt of Northeast Africa and Abjacent Areas. Vieweg and Sohn, Braunschweig, pp. 195–226.

Wahab, O.A., Afia, M.S., 1966. The lead–zinc deposits of Kutum. Sudanese Geology Survey Department Bulletin 14. Geological Survey Department of the Sudan, Khartoum, 47 pp.

Whalen, J.B., 1985. Geochemistry of an island-arc plutonic suite: the Uasilau–Yau Yau intrusive complex, New Britain. P.N.G. J. Petrol. 26, 603–632.